ISSN 1069-3513, Izvestiya, Physics of the Solid Earth, 2009, Vol. 45, No. 2, pp. 134–149. © Pleiades Publishing, Ltd., 2009.
Original Russian Text © D.M. Pechersky, B.Z. Asanidze, D.K. Nourgaliev, Z.N. Sharonova, 2009, published in Fizika Zemli, 2009, No. 2, pp. 49–65.

Petromagnetic and Paleomagnetic Characterization Deposits at Mesozoic/Cenozoic Boundary: The Tetritskaro Section (Georgia)

D. M. Pechersky[a], B. Z. Asanidze[b], D. K. Nourgaliev[c], and Z. N. Sharonova[a]

[a] *Schmidt Institute of Physics of the Earth (IPE), Russian Academy of Sciences, Bol'shaya Gruzinskaya ul. 10, Moscow, 123995 Russia, E-mail: diamar@front.ru*

[b] *Caucasian Institute of Mineral Resources (CIMR), Tbilisi, Georgia, E-mail: asanidze@mail.ru*

[c] *Kazan State University (KSU), Kremlevskaya ul. 18, Kazan, 420008 Russia, E-mail: danis.nourgaliev@ksu.ru*

Received July 2, 2007

Abstract—Petromagnetic and magnetostratigraphic characteristics are obtained for the Tetritskaro section. The boundary layer at the Mesozoic/Cenozoic (K/T) boundary is fixed primarily by an abrupt rise in the paramagnetic magnetization (total Fe concentration) and, to a lesser degree, by an increase in the concentration of such magnetic minerals as goethite, hemoilmenite, and magnetite. The along-section distribution of titanomagnetite of volcanic origin and metallic iron of cosmic origin does not correlate with the K/T boundary and lithologic properties of the sediments.

The boundary of the Mesozoic and Cenozoic geological eras lies within the reversed polarity chron *C29r* and is marked by an abrupt rise in the geomagnetic field paleointensity and an instability of paleomagnetic directions, rather than by a polarity change. The accumulation time of the boundary clay layer is about 1.5–2 kyr, while abrupt changes in the paleointensity and direction of the geomagnetic field encompass 30–40 kyr. Such long occurrence intervals of the events in question cannot be related to a short-term impact phenomenon.

PACS numbers: 91.25.Ng

DOI: 10.1134/S1069351309020049

INTRODUCTION

It is believed that the Mesozoic/Cenozoic (K/T) boundary was clearly reflected in long-scale surface and near-surface phenomena such as a significant biota extinction, powerful magmatic activity of plumes, impact events, and an increase in the magnetic susceptibility of oceanic and marine sediments at and/or near the K/T boundary [Veimarn et al., 1998; Alvarez et al., 1990; Ellwood et al., 2003; Ernst and Buchan, 2003; Grachev et al., 2005; Pechersky and Garbuzenko, 2005; Pechersky et al., 2006a, 2006b; and others]. On the other hand, analysis of continuous sections of oceanic sediments [Pechersky and Garbuzenko, 2005] showed that the K/T boundary coincides with a peak in the magnetic susceptibility χ only in 30% of studied cores. High values of the χ peak are usually confined to epicenters of epicenters of active plumes. The accumulation of magnetic material in sediments encompasses time intervals of a few tens of thousands of years (more often) to a few hundreds of thousands of years.

Until recently, only the behavior of the magnetic susceptibility of sediments at the K/T boundary was analyzed, while other magnetic properties were not studied. The relation of compositions and other characteristics of magnetic minerals in sediments to magmatic activity of plumes has not been studied at all. These deficiencies are being improved by detailed magnetolithologic and magnetomineralogical studies of outcrops on land of epicontinental sediments at the K/T boundary in sections of Volga region (Teplovka and Klyuchi) [Molostovsky et al., 2006], Austria (Gams) [Grachev et al., 2005; Pechersky et al., 2006], Mangyshlak (Koshak) [Pechersky et al., 2006a], and Georgia (Tetritskaro).

Anomalous behavior of the magnetic susceptibility in the K/T boundary layer is widespread in epicontinental sediments at least on a regional and possibly global scale and reflects specific features of accumulation of iron and magnetic minerals in the sediments. Two anomalous behavior patterns depending on the lithologic type of a section are known. The first pattern is characteristic of carbonate sediments of the Maastrichtian overlain by sandy–clayey deposits of the Danian: a sharp peak of the susceptibility is noted in the boundary layer and susceptibility values in the overlying Danian sediments are large than in the Maastrichtian deposits, as is observed, for example, in the sections Gams (Austria) [Pechersky et al., 2006b], Klyuchi (the Volga region) [Molostovsky et al., 2006], and Kubalach (Crimea) [Yampolskaya et al., 2004]. The second type is observed in carbonate and clay–carbonate deposits near the K/T boundary with thin interbeds of clays; in particular, a sharp peak of the susceptibility is confined to the K/T clay layer in such sections as Teplovka (the

Volga region) [Molostovsky et al., 2006], Koshak (Mangyshlak) [Pechersky et al., 2006a], Tetritskaro (Georgia) [Adamia et al., 1993], and Abat (Oman) [Ellwood et al., 2003].

The accumulation of iron hydroxides in the K/T boundary layer is likely a global phenomenon and can be due to geochemical, volcanic, and climatic processes and hydrothermal activity involving metal-bearing sediments [Gurvich. 1998]. This process differs significantly from terrigenous accumulation of magnetic minerals and, most importantly, must be of global nature.

Unlike iron hydroxides, accumulation of other magnetic minerals follows various patterns, evidently reflecting the origin of these minerals (cosmogenic spherules of metallic iron or volcanic grains of titanomagnetite) or local conditions of accumulation of terrigenous material (for example, magnetite, and ilmenite); a layered magnetic fabric of sediments is evidence of detrital deposition of both iron hydroxides and other magnetic minerals.

The Tetritskaro (Georgia) is an object of joint biostratigraphic, lithologic, geochemical, petromagnetic, and paleomagnetic studies at the IPE laboratory of geomagnetism, KSU paleomagnetic laboratory (Faculty of Geology), and CIMR paleomagnetic laboratory. This work discusses results derived from petromagnetic and paleomagnetic study of sediments of the Tetritskaro section.

BRIEF GEOLOGICAL CHARACTERIZATION OF THE OBJECT OF STUDY

A continuous sedimentary section including the K/T boundary is exposed in a ravine of a left tributary of the Khrami River, 500 m east of the village of Tetritskaro. The section contains Upper Cretaceous (Campanian–Maastrichtian) shallow marine sediments mostly consisting of limestones and clayey limestones and Paleocene shallow marine marls, clayey sandstones, clayey limestones, conglomerates, and breccias. Previously, a Tetritskaro section interval more than 20 m in thickness including the K/T boundary has been studied in detail (Fig. 1) [Adamia et al., 1993].

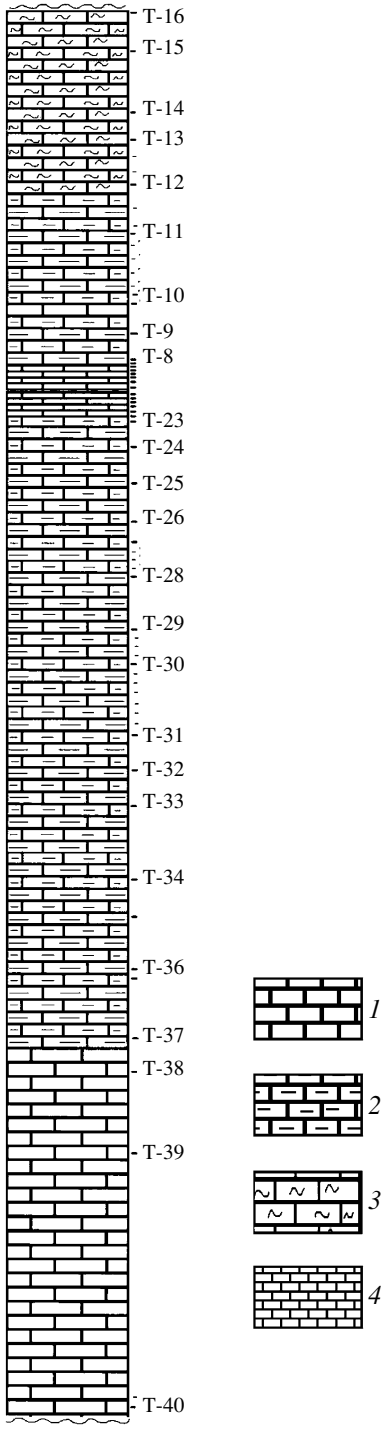

Fig. 1. Lithologic–stratigraphic column of the Tetritskaro section with indication of levels sampled for paleomagnetic and other studies: (*1*) light-colored limestones; (*2*) gray siliceous limestones; (*3*) brownish rose siliceous limestones; (*4*) boundary clays with the bold line showing the K/T boundary. The scale is 1: 20000.

Description of the Section (from bottom to top)

1. Maastrichtian. A 15-m thick group of beds of light-gray limestones. The carbonate fraction concentration is higher in the upper part of the group. The following zones are present in the group (from bottom to top): *Lithraphidites quadratus* (0–3.1 m); *Micula murus* (3.1–11.4 m); and *Micula prinstii*, the uppermost Maastrichtian zone (from 11.4 m to the boundary clay), with the complexes *Watznaueria barnesae, W. britanica, Arkhangelskielia cymbiformis, Prediscosphaera cretacea, Broinsonia enormis, B. parka, Eiffelithus turriseiffelli, Zigodiscus spiralis, Chiastozygus anceps, Cribrosphaerella ehrenbergii, Crepidolithus crenulatus, Parhabdolithus angustus, Micula murus, M. staurophora, M. prinsii, Markalius cyrkumradiatus, Tetralithus gothicus, Microrhabdulus decoratus, Lithraphidites carniolensis, L. quadratus, Lucian-*

orhabdus cayeuxii, Nephrolithus frequens. Representatives of the *Globotruncana contuse* zone are also found.

2. Boundary clay layer 1.5–2.5 cm thick (Fig. 1) resting directly on the Maastrichtian clayey limestones. A 1–3-mm thick rust-colored clay interbed occurs in the lower part of the clay layer. The clay layer contains shock-metamorphic quartz grains, and anomalously high of iridium (3.46–5.34 ng/g) have been fixed in the layer itself and at the base of its overlying limestones (a few millimeters thick). Occasional lenses and fragments of white limestone found in the layer are lithologically analogous to overlying limestones that contain nannofossil complexes characteristic of the lowermost Danian, the zones of *Biantholithus sparsus: Braarudosphaera bigelowii, B. turbinea, B. discula, B. africana, B. irregularis, Biantholithus sparsus, Thoracosphaera operculata, T. saxea, Biscutum parvulum, Placozygus sigmoides, Cyclagellosphaera reinharditii, Marcalius inversus, M. apertus.* Occasionally, clay fills microdistributive fissures. Adamia et al. [1993] admit that, as a result contamination, limestones resting on the boundary clay layer can contain iridium or shock-metamorphic quartz grains.

3. Paleogene, Danian: light-gray and white limestones 0.8–0.9 m thick. Thin interbeds and lenses of calcareous clay varying in thickness from 0.5 to 10 mm are noted in the lower part of the interval.

4. Light-gray and gray clayey limestones 0.8–1 m thick, a zone of *Biantholithus sparsus*.

5. Gray and light-brown gray limestones 0.8–2 m thick, a zone of *Cruciplacolithus tenius.*

6. Brown gray, red gray, and gray clayey limestones and marls 2.4 m thick. The following zones have been documented: *Cruciplacolithus tenius* (0–1 m), *Chiasmolithus danicus* (1–2.1 m), and *Cyclococcolithus robustus* (2.1 m and higher).

The rocks are characterized by a nearly monoclinal, shallow-angle occurrence: the sediments dip northeastward at angles of 10–20° (mostly at 15°), and the dip azimuth is 35–40° in the upper part of the Maastrichtian deposits and in the Danian deposits and 50–60° in the middle and lower parts of the Maastrichtian. Accordingly, the fold test is actually inapplicable to the section.

Oriented samples for paleomagnetic examination and specimens for a complex of petromagnetic and other studies were taken from a section interval of an overall thickness of 31 m including 22 m below and 9 m above the boundary clay layer.

METHODS OF PETROMAGNETIC AND PALEOMAGNETIC STUDIES

Two-cm cubes sawn from oriented hand samples were used for paleomagnetic measurements, as well as for measuring the magnetic susceptibility and standard isothermal petromagnetic characteristics (after alternating field (AF) demagnetization); sample pieces less than 1 cm in size were subjected to thermomagnetic analysis. Since the sizes of the cubes and particularly the smaller sample pieces were not strictly controlled, the measured values were related to the sample weight; i.e., the specific susceptibility and the specific magnetization were determined.

The petromagnetic studies included measurements of the specific magnetic susceptibility χ, hysteresis characteristics, and the anisotropy parameters A_χ and A_{rs}. The susceptibility and remanence were measured with a KLY-2 susceptibility bridge and JR-4 magnetometer, respectively, and hysteresis characteristics of samples were examined with the use of a coercivity spectrometer [Burov et al., 1986; Yasonov et al., 1998] providing curves of isothermal magnetization of up to 0.5 T in an automatic mode. The measured magnetization curves were used for determining the specific saturation remanence M_{rs}, saturation maggnetization without the paramagnetic+diamagnetic component M_s, coercivity without the effect of the paramagnetic+diamagnetic component H_c, and remanent coercivity H_{cr}. The ratios of the hysteresis parameters H_{cr}/H_c and M_{rs}/M_s can be used for estimating the domain state of magnetic grains [Day et al., 1977].

The magnetization of paramagnetic+diamagnetic components was estimated from magnetization curves in a field above the saturation of magnetic components of samples, namely, in a field of 500 mT. If the saturation field could not been attained, the resulting values of the paramagnetic magnetization were possibly overestimated [Richter and van der Pluijm, 1994].

Thermomagnetic measurements were made with an express Curie balance [Burov et al., 1986] (the dependence of the induced magnetization on temperature was measured at a heating rate of 100°C/min). Such a high heating rate was possible due to a high sensitivity of the instrument and enables the use of very small samples (less than 0.2 g in weight). The temperature gradient in such small samples does not exceed 10°C. The thermomagnetic analysis was conducted in a constant magnetic field of 200 mT; this is the saturation magnetization M_s for such magnetic minerals as magnetite, hemoilmenite, and iron; in several samples, the saturation field is higher in some grains of hemoilmenite and such iron hydroxides as goethite possessing weak ferromagnetism, so that an induced magnetization was actually measured. Curves $M_i(T)$ of the first and repeated heatings to 800°C were obtained for all samples. The concentrations of magnetite, iron, hemoilmenite, titanomagnetite, and goethite in samples were estimated; for this purpose, the contribution of a given magnetic mineral to the M_i value was determined from the curve $M_i(T)$ and the resulting value was divided by the specific saturation magnetization of this mineral. According to [Nagata, 1961], the following values of M_s were accepted: 90 A m^2/kg for magnetite, for titaniferous magnetite 80, 200 A m^2/kg for iron, and 4 and

10 A m^2/kg for hemoilmenite at $T_c > 300$°C and $T_c \approx$ 250–260°C, respectively. Data from [Bagin et al., 1988] used for goethite ($T_c \le 150$°C) and titanohematite (T_c = 630–670°C) imply that the specific saturation magnetization in these minerals varies from 0.02 to 0.5 A m^2/kg depending on their aggregate state. Judging from well-defined Curie points, the titanohematite are in a fully crystalline state and the value M_s = 0.5 A m^2/kg is accepted for them. We accepted M_s = 0.25 A m^2/kg for goethite by analogy with data from the Gams section presented in [Grachev et al., 2005], where results of petrographic and chemical analysis of rocks are described. Apart from hemoilmenite and titanomagnetite, the samples contain grains of ilmenite, which is paramagnetic at room temperature; consequently, the resulting estimate of the hemoilmenite concentration is a lower bound for the overall concentration of hemoilmenite and ilmenite in the samples studied. The value M_s = 0.25 A m^2/kg we accepted for goethite is optimal, but even this estimate is a lower bound for the concentration of iron hydroxides because they also include paramagnetic varieties and, moreover, the saturation field of fully crystalline goethite is higher than the magnetic field of the thermomagnetic analysis. Of course, the estimates obtained for concentrations of magnetic minerals are rather tentative, but their relative values correctly reflect the actual pattern.

Values of the paramagnetic (M_p) and diamagnetic (M_d) magnetizations provide constraints on the fractions of paramagnetic (paramagnetic iron hydroxides, clays, etc.) and diamagnetic (carbonates and quartz) minerals in sediments. If the paramagnetic magnetization at room temperature is known, the paramagnetic magnetization at 800°C can be easily calculated with the help of the Curie–Weiss law. Diamagnetic magnetization depends on temperature very weakly [Vonsovskii, 1971]. Since all measurements are made in the same external magnetic field of 500 mT or reduced to such a value (in these cases, we accept a linear dependence of the paramagnetic and diamagnetic magnetizations on the field), the diamagnetic and paramagnetic magnetization components at room temperature can be calculated from simple equations:

$$M_p + M_d = M_{20},$$
$$0.274M_p + M_d = M_{800}.$$

Hence we have $M_p = 1.377(M_{20} - M_{800})$, where M_{20} is determined from the curve of isothermal magnetization of a sample at room temperature in a constant magnetic field of 500 mT, which is higher than the saturation field of magnetic minerals present in the sample, and M_{800} is the sample magnetization at 800°C. The factor 0.274 is the temperature ratio 295K/1075K (the Curie–Weiss law).

Paramagnetism of samples is actually controlled by the Fe concentration in paramagnetic minerals, so that the value M_p can provide an idea of the overall Fe concentration in rocks.

To gain additional constraints on the composition of magnetic minerals, we obtained thermomagnetic curves of successive heatings of samples to different temperatures; this allowed us to trace mineralogical alterations that occurred in samples during the heatings and to distinguish them from Curie points.

Paleomagnetic studies included (a) measurements of the value and direction of the natural remanent magnetization (NRM); (b) its removal in alternating magnetic fields (*H*-demagnetization) up to 40 mT at step of 5 mT; (c) NRM removal by heatings (*T*-demagnetization) from25°C to 400°C (75, 100, 125, 150, 175, 200, 225, 250, 275, 300, 350, and 400°C); and (d) calculation of the stable NRM component (20–30 mT after the *H*-demagnetization) to NRM (M_n/M_{rs}), characterizing the relative paleointensity. The presence of a M_n/M_{rs} minimum is evidence for the absence of an appreciable break at the boundaries of magnetic zones of opposite polarities, whereas the position of the minimum gives additional constraints on the position of the boundaries of the magnetic zone *C29r*.

PETROMAGNETIC RESULTS

Magnetization of rocks (Table 1). Values of the specific magnetic susceptibility (χ), specific saturation magnetization M_s, and specific saturation remanence M_{rs} vary within narrow limits except for two horizons (brown clays in the boundary layer and Danian marls relatively enriched in magnetic minerals, samples t11–t13), which is evidence of a rather homogeneous composition of the rocks (mainly clayey limestones) and a relatively low magnetization of the limestones (samples t1–t10). Positive correlation between M_s and M_{rs} (Fig. 2a) points to a decisive role of the concentration of magnetic minerals in both magnetizations. The correlation between M_s and the susceptibility is much weaker (Fig. 2b), which can be naturally attributed to an appreciable contribution of paramagnetic and diamagnetic material to the susceptibility that is absent in M_s and magnetic minerals contribute to the susceptibility more significantly in the range of relatively large values of M_s and χ. On the contrary, a very strong positive correlation is observed between the susceptibility and paramagnetic magnetization (Fig. 2c). As seen from Fig. 2c, two groups of points can be distinguished: (1) the main group including the majority of samples (limestones and marls) and characterized by a predominant contribution of paramagnetic and diamagnetic material to the susceptibility and (2) a small group of boundary clay layer samples enriched in paramagnetic material. These two groups also differ in relationships between M_d and χ: (1) M_d changes sharply with small variations in χ (the left part of the plot in Fig. 2d), a distinct negative correlation exists between M_d and χ, and the contribution of diamagnetic material to χ is noticeable; and (2) χ varies significantly with small changes in M_d, which can be attributed to a rise in the χ contribution of paramagnetic material (the right-hand part of

Table 1. Magnetic properties of sediments of the Tetritskaro section

Sample	Distance, cm	χ	M_p	M_d	M_s	M_{rs}	A_{rs}	H_{cr}	H_c
t16	880	2.67	7.08	–1.36	0.862	0.224	1.07	50.4	15.2
t15	780	2.06	5.607	–1.35	1.008	0.227	1.04	60.2	16.5
t14	630	2.63	7.03	–1.63	0.902	0.246	1.07	48	12.7
t13	560	3.23	7.96	–0.374	1.784	0.31	1.11	39.3	10
t12b	470	1.76				0.324			
t12a	450	1.44				0.462			
t12	440	4.26	7.72	–1.14	2.544	0.396	1.06	35.1	8.94
t11b	365	2.63				0.669			
t11a	345	1.11				0.574			
t11	340	3.94	6.14	–1.41	1.562	0.253	1.07	34.9	8.95
t10e	275	1.4				0.174			
t10d	265	1.4				0.138			
t10b	225	2.2				0.12			
t10a	220	1.42				0.079			
t10	210	1.68	5.69	–1.85	0.364	0.058	1.05	32.3	11.5
t9	110	1.1	6.146	–2.1	0.348	0.054	1.02	29.5	8.69
t8	70	0.81	4.56	–2.51	0.425	0.034	1.11	33.1	8
t6	40	0.78	4.83	–2.286	0.229	0.04	1.21	32	10.2
t5	30	0.82	4.53	–2.42	0.416	0.035	1.08	31.2	7.68
t4a	20	0.81				0.029	1.11		
t4	19	0.82	4.46	–2.24	0.145	0.031	1.02	30.9	12.4
t3-3	18	1.42	3.81	–1.33	0.286	0.03		34.2	8.3
t3-1	16	0.81	4.47	–1.93	0.221	0.018	1.13	32.7	8.6
t2-1	10.5	0.69	3.76	–1.73	0.746	0.041	1.01	28.1	4.84
t1-4	9.5		4.67	–1.83	0.368	0.032		33.9	8.8
t1-1	2	1.29	5.34	–1.16	0.7	0.04	1.02	29.7	5.9
Brown clay 1	0		39	–0.7	2.62	0.222		29.6	7.26
Brown clay 2	0		57.1	–0.67	3.86				
Gray clay	0	8.33	14.88	–0.08	1.01	0.067			
White clay	0		13.37	–0.07	0.91				
Clay mixture	0	9.15				0.13			
t17-1d	–1	2	6.78	–0.63	0.46	0.025		30.5	5.93
t17-2	–2	1.78	7.84	–0.96	0.269	0.023	1.08	32	7.5
t17d	–2		6.84	–0.69	0.33	0.03		31.8	7.3
t17-3	–3		7.86	–0.71	0.058	0.022		31.8	9.5
t17-4d	–4		6.51	0.15	0.281	0.025		31.5	6.9
t18-1d	–5		6.9	–1.86	0.111	0.02		29.8	8.2
t18	–7	1.49	7.56	–2.06	0.264	0.052	1.05	36.6	8.84
t19-1	–9	2.02	7.83	–0.91	0.557	0.063	1.12	37.8	8.43
t19-2d	–11		8.11	–0.15	0.241	0.05		36.2	9.7
t20	–13	2.01	6.52	0.85	0.338	0.032	1.12	32.3	6.27
t21	–15	2.06	7.17	–0.58	0.366	0.041	1.07	33.7	8.65
t22	–20	2.11	6.81	–0.01	0.434	0.04	1.08	32.9	8.1
t23	–40	1.88	7	–0.14	0.257	0.041	1.2	30.7	9.2
t24	–90	3.24	4.22	–2.45	0.477	0.034	1.17	27.7	6.1

Table 1. (Contd.)

Sample	Distance, cm	χ	M_p	M_d	M_s	M_{rs}	A_{rs}	H_{cr}	H_c
t25	–170	2.66	8.54	0.88	1.002	0.143	1.1	65.2	11.7
t26	–270	3.12	9.47	–0.04	0.12	0.068	1.08	35	12.2
t27	–320	2.84				0.068	1.16		
t27a	–345	3.95				0.085			
t27b	–372	3.16				0.122			
t28	–390		9.94	0.355	0.69	0.086		35.3	9.9
t28a	–490	3.32				0.067	1.14		
t29	–590	4.28				0.034	1.07		
t29a	–600	3.32				0.172			
t29b	–610	2.68				0.088			
t29c	–615	2.68				0.177			
t30	–650	2.48	7.48	0.47	0.245	0.049	1.06	31.9	10.1
t30a	–680	2.63							
t30b	–685	2.47				0.093			
t30c	–715					0.1			
t30d	–765	1.89				0.162			
t30e	–795	2.16				0.081			
t30f	–845	3				0.27			
t32	–900	2.71				0.044	1.13		
t33	–970	3.74	8.6	1.07	0.422	0.07	1.25	38.5	10.8
t34	–1170	2.99				0.056	1.21		
t34a	–1270	2.38	5.65	2.21	0.622	0.072	1.19	41.6	10.8
t35	–1370	2.3	7.32	0.5	0.289	0.055	1.23	32.3	11.5
t36	–1470	2.06	6.96	–0.27	0.446	0.059	1.08	32	7.84
t37	–1620	3.05	7.96	0.19	0.608	0.109		46.9	13.4
t38	–1670	3.46	9	0.78	1.15	0.19	1.18	51.6	14.2
t39	–1800	2.56	8.14	0.92	0.643	0.064	1.22	33.8	8.42
t40	–2200	1.77	6.48	–0.81	0.58	0.077	1.13	37	11.3

Note: The second column characterizes the position of a sample in the section measured from the boundary clay; χ is the specific magnetic susceptibility (10^{-8} m^3/kg); M_p and M_d are, respectively, paramagnetic and diamagnetic magnetizations in a field of 500 mT (10^{-3} A m^2/kg); M_s and M_{rs} are, respectively, saturation magnetization and saturation remanence (10^{-3} A m^2/kg); A_{rs} is the anisotropy of the saturation remanence; and H_c and H_{cr} are, respectively, coercivity and remanent coercivity (mT).

the plot in Fig. 2d), and a large scatter in M_d and a weak correlation of M_d with χ are observed.

A decisive role of paramagnetic material in χ is evident from nearly coinciding along-section behavior patterns of χ and M_p (Figs. 3a, 3d). The along-section distributions of magnetic minerals and carbonate (diamagnetic) material are also similar, as is seen from the behavior of M_s, M_{rs}, and M_d) Figs. 3b, 3c, 3e).

The behavior of the paramagnetic magnetization shows that Fe concentration in paramagnetic compounds varies only slightly along the section: its level is somewhat higher in the Maastrichtian deposits due to a larger fraction of terrigenous clayey material in them. Accordingly, the Maastrichtian and Danian intervals of the section differ sharply in diamagnetic magnetization (Fig. 3e): it is highest in "pure" limestones of the lower Danian (t1–t10) and is so smaller than the paramagnetic component that it cannot be extracted. This is not surprising because the paramagnetic magnetization of natural minerals is two to three orders higher than the susceptibility of diamagnetic minerals [Rochette et al., 1992].

Against the rather homogeneous along-section distributions of magnetic, paramagnetic, and diamagnetic material, the boundary clay layer is sharply distinguished by a higher susceptibility, saturation magnetization, and paramagnetic magnetization (Fig. 3), i.e.,

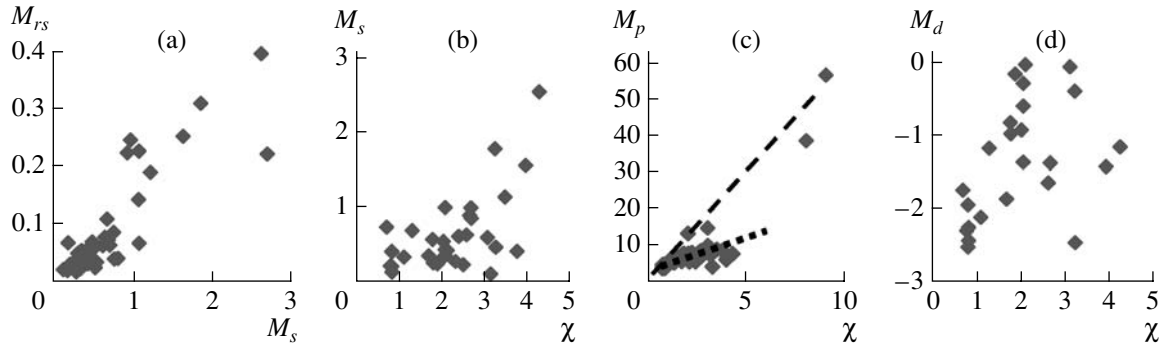

Fig. 2. Correlations between M_s, M_{rs}, χ, M_p, and M_d.

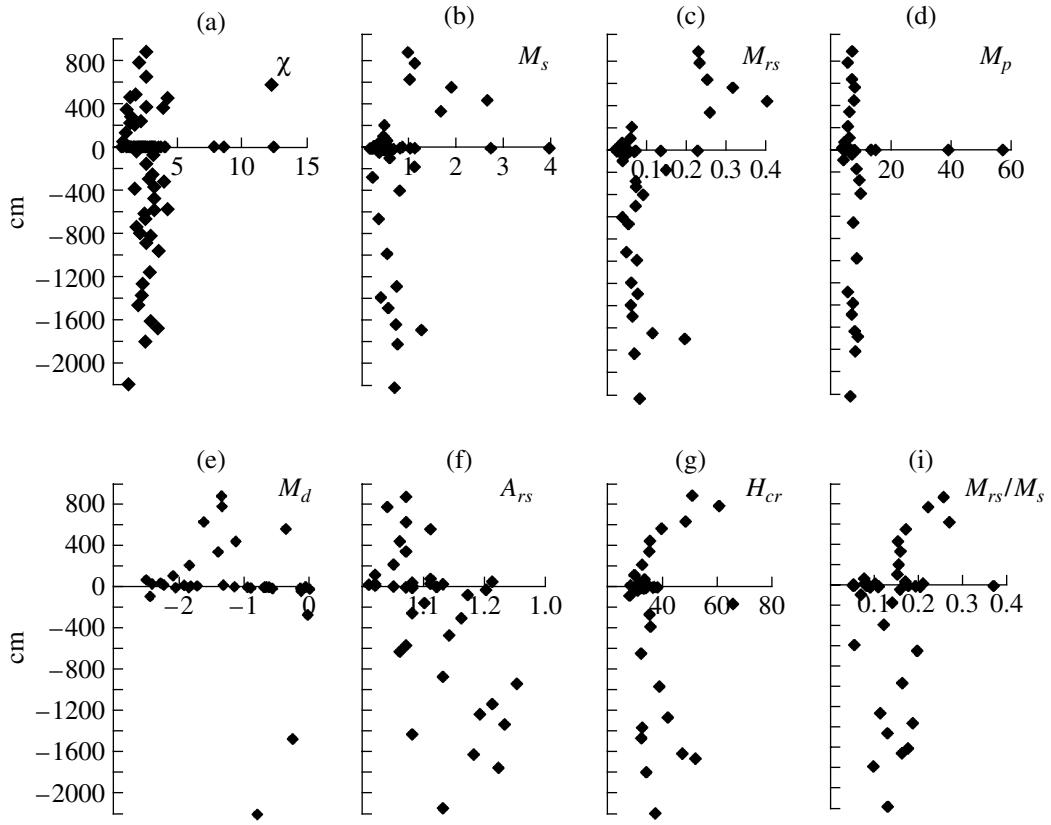

Fig. 3. Along-section distributions of the main magnetic characteristics: (a) specific magnetic susceptibility χ (10^{-8} A m^2/kg); (b) specific saturation magnetization M_s (10^{-3} A m^2/kg); (c) specific saturation remanence M_{rs} (10^{-3} A m^2/kg); (d) specific paramagnetic magnetization M_p (10^{-3} A m^2/kg); (e) specific diamagnetic magnetization M_d (10^{-3} A m^2/kg); (f) saturation remanence anisotropy A_{rs}; (g) remanent coercivity H_{cr} (mT); (i) ratio M_{rs}/M_s.

primarily by a higher Fe concentration in paramagnetic and weakly ferromagnetic varieties.

Now we address magnetic characteristics reflecting the composition (data of thermomagnetic analysis), size and structure of magnetic minerals (hysteresis parameters), and conditions of their accumulation in sediments (magnetic anisotropy).

Composition of magnetic minerals. To estimate compositions of magnetic minerals, we used data of thermomagnetic analysis (*TMA*). Because of a large value of the paramagnetic component, the curves $M(T)$ are often of a nearly hyperbolic shape (Fig. 4) and, for limestones (t1–t10) above 600–700°C, extend into the region of negative values, evidently due to diamagnetic

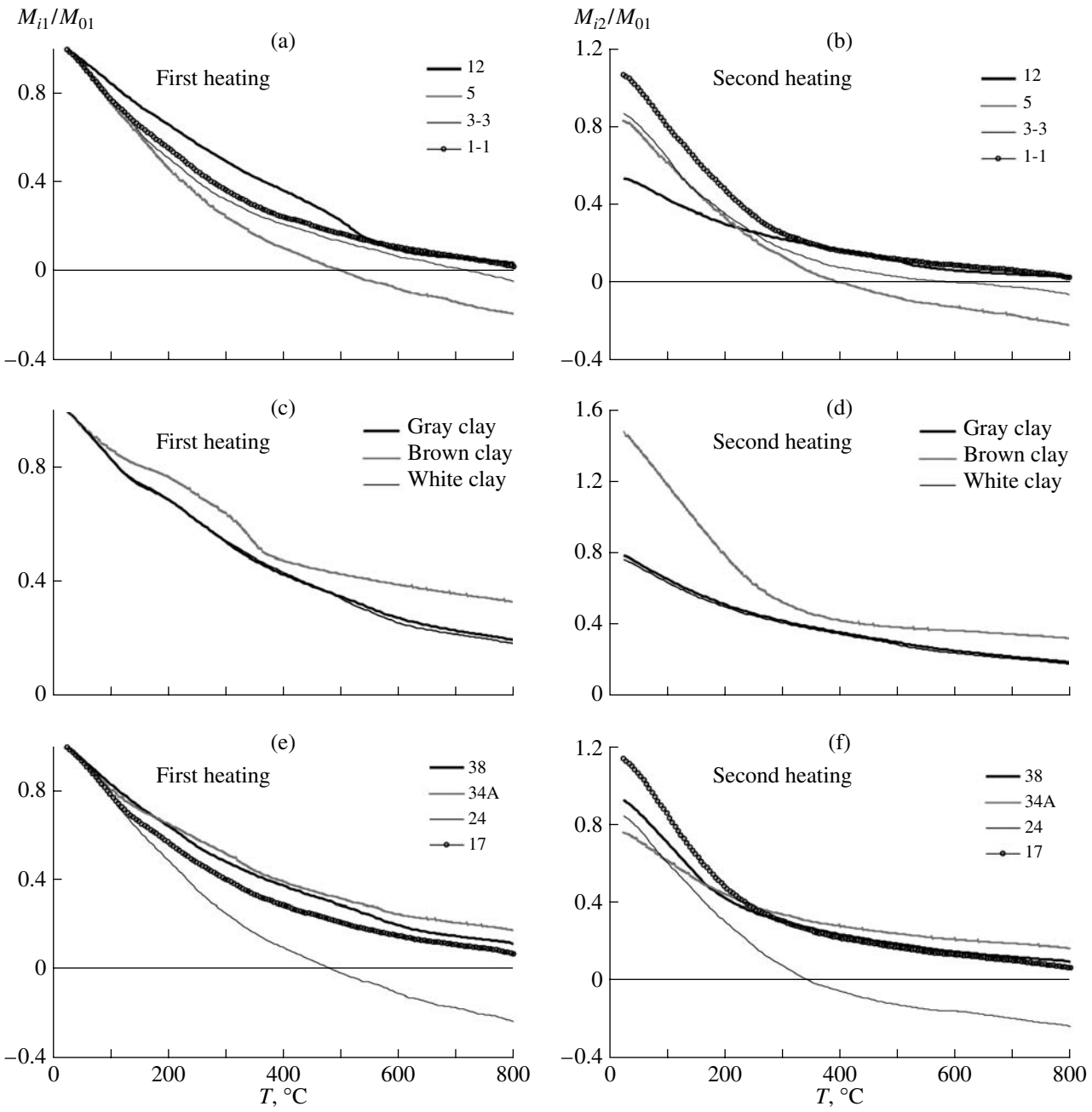

Fig. 4. Examples illustrating the TMA results.

carbonates. Against this background, the following magnetic phases are recognizable (Table 2).

(a) T_c = 100–180°C. The phase is fixed in all samples and accounts for 5–20% of magnetization. In the majority of cases, this phase is destroyed during heating. Evidently, this is a mixture of iron hydroxides of the goethite type. Their concentration varies mostly from 0.1 to 0.5% and only in the marls, having larger values of M_s and M_{rs} (Fig. 2), rises to 0.7–0.9%; the goethite concentration in the boundary layer clay varies from 1 to 2,8%, attaining a maximum in the brown clay enriched in iron hydroxides (Fig. 5). Goethite correlates most strongly with the magnetic susceptibility and paramagnetic magnetization.

A phase with T_c = 120–150°C is preserved in eight samples upon their heating to 800°C. This is neither goethite nor iron hydroxides at all but a very stable mineral, possibly Fe–Mg–Al ferrospinel. It is more likely that this is a secondary mineral forming during laboratory heating of samples to high temperatures [Bagin et al., 1976, 1977; Gapeev and Tselmovich, 1988].

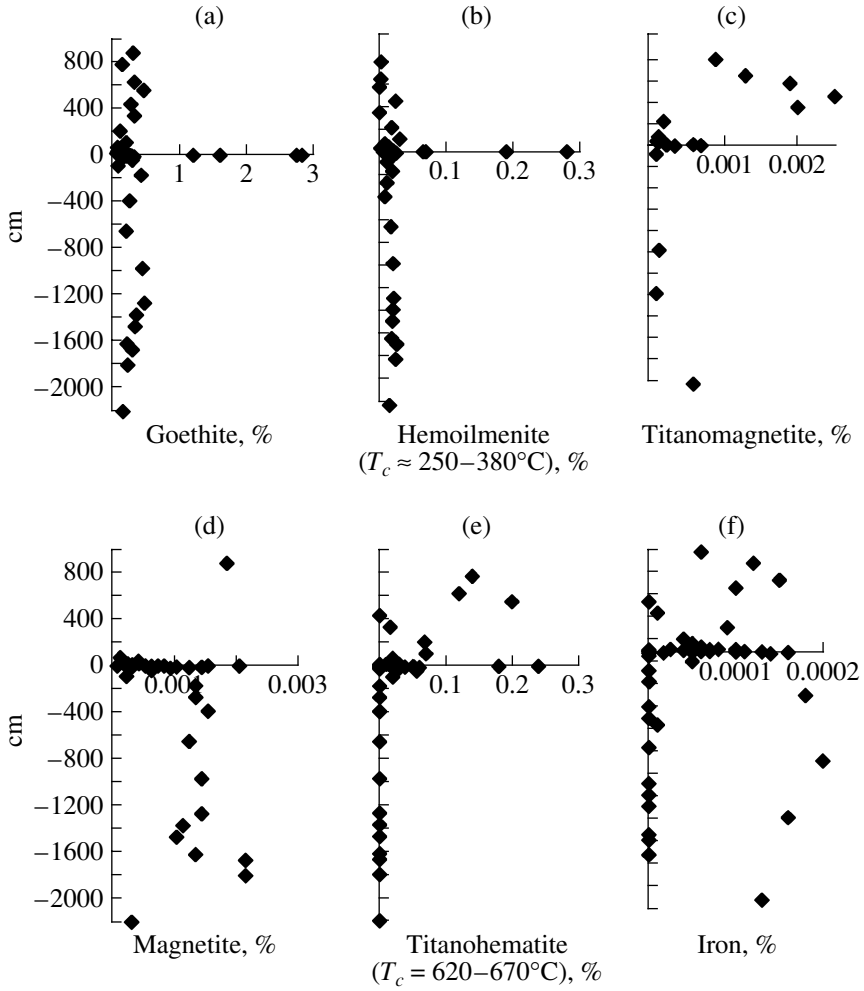

Fig. 5. Along-section distributions of magnetic minerals: (a) goethite; (b) hemoilmenite; (c) titanomagnetite; (d) magnetite; (e) titanohematite; (f) metallic iron. The concentrations are given in mass percents.

(b) T_c = 250–380°C. These magnetic phases fixed in the majority of samples account for 10–70% of magnetization and are stable with respect to heating. Moreover, upon heating to 800°C, the relative contribution of the phase with T_c = 250–300°C increases and this phase arises even in samples in which it was not fixed during the first heating (Table 2). The phases with T_c = 250–300 and 310–380°C are often distinguished rather tentatively because they cannot be separated against a hyperbolic curve $M(T)$. Apparently, they form a continuous series of solid solutions (probably, hemoilmenites [Pechersky et al., 2006]. If their saturation magnetization is set at ~4 A m^2/kg, the concentration of hemoilmenites in the Tetritskaro rocks varies mainly from less than 0.001 to 0.03%, reaching 0.28% only in the boundary layer clay (Fig. 6). It is likely that goethite and hemoilmenite were concurrently accumulated (Fig. 5).

(c) T_c = 500–550°C. This phase occurs in many samples in two variants: either the phase with T_c = 500–550°C is fixed during the first heating, or it arises during the second heating due to partial homogenization of magnetite grains, i.e., the phase is titanomagnetite in this case (Table 2). The titanomagnetite accounts for 10–60% of magnetization and, accordingly, its concentration varies from less than 0.0001 to 0.0025% (Fig. 5). The along-section distribution of titanomagnetite correlates mainly with M_s, M_{rs}, and NRM, implying its predominant contributions to these magnetizations. Titanomagnetite is not discovered in the boundary layer, while its concentrations are highest in the ~340–630-cm interval of the Danian limestones (Fig. 5); i.e., lithologic control of the titanomagnetite distribution is absent.

(d) T_c = 570–610°C The phase is fixed in the majority of samples during their first heating and is evidently magnetite that partially subjected to single-phase oxidation ($T_c \geq 590$°C). The magnetization in most samples decreases due to partial destruction (oxidation) of magnetite and titanomagnetite and homogenization of the latter (Table 2); we have M_1/M_o = 0.54–0.9, and rare ratio values of 1–1.48 are evidently caused by a rise in magnetization due to formation of more magnetic

hemoilmenite with a Curie point below 300°C [Nagata, 1965], whose effect is stronger than the aforementioned magnetization decrease. Magnetite accounts for 5–30% of magnetization, and its concentration varies from less than 0.0001 to 0.002%; magnetite is present in Maastrichtian sediments, occurs in very small concentrations at the base of the Danian, and is virtually absent in the overlying Danian limestones. Its concentrations are highest in clays of the boundary layer (Fig. 5); i.e., unlike titanomagnetite, lithologic control of the along-section distribution of magnetite is noticeable.

(e) T_c = 620–670°C The phase is present in many samples of the Danian deposits but much more rarely in Maastrichtian sediments (Table 2). In some samples, this phase is preserved after heating to 800°C; i.e., it is rather stable. In several samples, it is destroyed after the first heating but a phase with $T_c < 300$°C arises; finally, there are samples in which this phase arises after the first heating to 800°C. In all these cases, we classify it as titanohematite. This mineral, more specifically, a series of solid solutions, is quite insensitive to heating in air, i.e., in an oxidizing medium, and is represented in part by intergrowths with and lamellae in ilmenite; such aggregates are partially or completely homogenized. In the third, the phase is likely a product of oxidation of titanomagnetite and magnetite and dehydration of iron hydroxides. Titanohematite accounts for 5–30% of magnetization. Accepting its saturation magnetization of ~0.5 A m^2/kg, we find that its concentration varies from 0 in the Maastrichtian sediments, where titanohematite is present only in their uppermost part, to 0.2% in the boundary layer and Danian deposits (Fig. 5). The distribution of titanohematite is independent of lithologic characteristics of the section and apparently points to oxidation conditions that existed in the sediments at their deposition stage; i.e., the Danian sediments deposited under higher oxidation conditions compared to the Maastrichtian sediments.

(f) T_c = 710–790°C. The phase is fixed in many samples but is more widespread in the Danian deposits (Table 2). It is metallic iron with minor impurities. After heating, it is often destroyed (oxidized) and is better preserved in limestone samples (t1–t10). Iron accounts for 5–20% of magnetization; accordingly, its concentration varies from 0 to 0.0002% and it correlates with neither concentrations of other magnetic minerals nor lithologic characteristics of the section (Fig. 5). Metallic iron is not discovered in the boundary clay layer.

Magnetic anisotropy. The magnetic susceptibility anisotropy varies within narrow limits and does not exceed 1.05; i.e., paramagnetic and diamagnetic minerals (primarily, iron hydroxides, contributing most to the susceptibility and bringing about strong anisotropy) do not form in sum a foliation or lineation. Anisotropy of the saturation remanence (A_{rs}), determined solely by magnetic minerals, varies within wider limits, from isotropic values (less than 1.05) to 1.21–1.25 (Table 1).

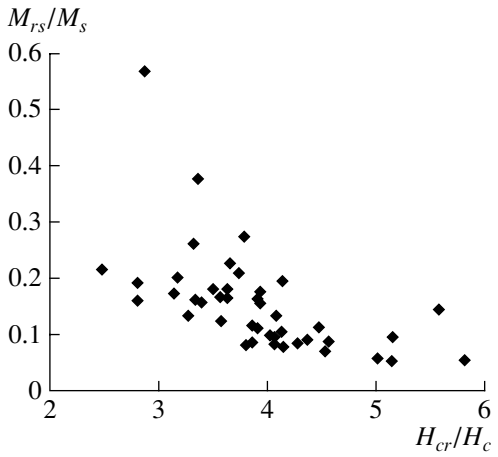

Fig. 6. Diagram of H_{cr}/H_c versus M_{rs}/M_s (Day plot diagram) [Day et al., 1977].

The value A_{rs} correlates with neither compositions nor concentrations of magnetic minerals (cf. Figs. 3 and 5). Relatively anisotropic samples generally possess a planar magnetic fabric, indicating terrigenous accumulation of magnetic minerals. A general tendency to a decrease in A_{rs} toward shallower depths is observed (Fig. 6). Apparently, the degree of compaction of the sediments and the amount of terrigenous admixtures in limestones vary, to some extent, along the section. Thus, anisotropy is relatively weakest in the "purest" Danian limestones, characterized by the highest diamagnetic magnetization, whereas anisotropy is strongest in clayey limestones and marls of the Maastrichtian, which have a higher paramagnetic magnetization as compared with the Danian limestones (Fig. 3).

Coercivity of magnetic minerals. Except for the upper horizon, where H_{cr} = 50–60 mT and M_{rs}/M_s = 0.26–0.27, the coercivity of the rocks is rather uniform: the majority of samples have H_{cr} = 30–40 mT and M_{rs}/M_s = 0.1–0.2 (Table 1, Fig. 6). Judging from the H_{cr} and M_{rs}/M_s values, nearly single-domain and pseudo-single-domain magnetic grains prevail in the rocks; however, the vast majority of points in the Day diagram (Fig. 6) lie in the multidomain area, which is evidently due to a large amount of superparamagnetic grains [Dunlop, 2002a, 2002b]. In strong fields, their effect on M_s can be eliminated as paramagnetism disappears (provided that the superparamagnetic grains are very fine). In a weak field (of an order of H_c), the susceptibility of these grains is high and this is why they are remagnetized in a field appreciably smaller than the real value of H_c. Therefore, the H_{cr}/H_c values are overestimated. The superparamagnetic curve is not linear, as in the case of paramagnetic material (at room temperature), but hyperbolic, typical of ferri- and ferromagnets. Removing the paramagnetic magnetization by linear approximation, we do not eliminate the superparamagnetic component in M_s, which is absent in M_{rs}.

Table 2. TMA results from Tetritskaro samples

Sample	Distance, cm	First heating, Curie point (percentage in the M value)							Second heating, Curie point (percentage in the M value)							M_t/M_o
		Goethite, FS (?)	HI	TH	TM	MT	TH	Fe	FS	HI	HI	HI	MT	TH	Fe	
t16	880	140(10)				600(60)		790?		280			600?			0.65
t15	780	150(5)			550(35)		640(30)	790(10)		290				650		0.74
t14	630	150(10)			580(40)		640(20)	760(10)		280		560		660		0.63
t13	560	130(10)			590(40)		650(30)	730(5)		260		560?				0.6
t12	440	150(5)		320?(20)	550(45)					220		540				0.54
t11	340	150(15)			550(60)	610?				220		530				0.67
t10	210	110(5)	270	360(45)	500(10)		640(20)	730(10)			390	530				0.77
t9	110	120(10)	300(70)				650(20)	770(5)		300		555		630	780	0.72
t8	70	100(5)	260	360(35)	520(10)	590?(10)	645	740		270	370	510		670	770	0.82
t6	40		290	350(50)	490	580(30)	630(10)	730(10)		270	360		580		740	0.81
t5	30	100?(5)		320	550		620	710(<5)		270	370	530		670	720	0.84
t4	19	100(<5)	270	380(50)		570(20)	650(5)	760(5)			360		570	650	760	0.8
t3-3	18	150(10)	300	360(45)	610(25)		670	770(<5)	150	290	380	480		610	680	0.81
t3-1	16	150(5)	280	380			670	740(<5)	130	250	360		560	640	730	0.83
t3	17	100(<5)	290	370(60)	560?			745(20)		260	390	470		560	745	0.85
t2-1	10.5	130(5)		310(40)				730(<5)		290	350		570?		730	0.82
t1-4	9.5	120(10)		330(50)		590(15)		750(5)			330				750	0.68
t1-1	2	100(10)		360(40)		580(25)		780(10)		290	390		570?		780	1.07
Brown clay 1	0	140(15)		350(40)		590	660			280				670		0.94
Brown clay 2	0	130(10)	260	370(30)		570?	660?			270				670		1.48
Gray clay	0	130(20)	260	360(40)		580(10)		710??		260			580			0.8
White clay	0	120(15)	250	350(20)	520	600(15)				250		520				0.77
t17-1	–1	100	280?	330?	580?			750(5)		270	350	530			740	0.75
t17-2	–2	150(5)	290(10)			590(50)		730(5)		280			590		740	0.72
t17	–2	150(10)		360(30)	530?(20)		630(10)	790(5)		290			570			1.13

Table 2. (Contd.)

Sample	Distance, cm	First heating, Curie point (percentage in the M value)							Second heating, Curie point (percentage in the M value)							M_t/M_o
		Goethite, FS (?)	HI	TH	TM	MT	TH	Fe	FS	HI	HI	HI	MT	TH	Fe	
t17-3	–3	130(10)	290(25)	350?		590		740?		280	350	520?				0.74
t17-4	–4	100(10)		390?	590		660	740?			400?	530			740	0.81
t18-1	–5	120(5)	300(30)	380	500	600		750(<5)		270	570			640		0.77
t18	–7	120(10)	300(30)	360?		590		740?		290?	360?				740?	0.75
t19-1	–9	180(10)		370(25)	610(30)			740?	120	260	370	550			740	0.77
t19-2	–11	120(5)	260?	360?	510?	600				270?		530		670		0.78
t20	–13	200?	280?	360(30)		620		720?	150	280	370			590	760?	0.8
t21	–15	180(10)	280	370(20)	600(40)				120	260	370	550				0.79
t22	–20	130(10)	300(30)	360		600(30)		730?		270	360			600?	730	0.87
t23	–40	130(10)	280?	360(30)	590(20)		660			280?	360	550			760	0.84
t24	–90	100?	260	360(50)	500?	600(20)	660	740(<5)		260	350	560		650	720?	0.85
t25	–170	120(10)	270?	370?(20)		600(30)				270?	350		560	660		0.74
t26	–270		250(30)	340?		600(30)			150	250	360		580		730	0.76
t28	–390	150(5)	250(20)			590(30)		740(<5)	150	270?			560?			0.73
t30	–650	100(5)	280(20)			590(20)		750(<5)		280?				590	740	0.76
t33	–970	110(10)	290(20)	360?	600(30)			750(<5)		270?		510?		580		0.77
t34a	–1270	120(10)		360(20)		600(30)					340?		560?			0.76
t35	–1370	150(10)	270?	350(25)		590(30)				260	360		560		770?	0.9
t36	–1470	150(10)	280(20)	340?		590(30)		740?	150	260	370			590	700?	1.005
t37	–1620	110(5)	270	360(20)		600(30)				280?	350					0.83
t38	–1670	110?(5)	260(20)			580(35)				200	350?			580?		0.92
t39	–1800	110(5)	270?	350(25)		590(20)				260?	350?					0.82
t40	–2200	100(5)	270(15)	360(10)	600(10)			740(<5)		270?	380?	460				0.82

Note: The Curie points after the first and second heatings are given together with the value (in parentheses) of the contribution of a given magnetic phase to the magnetization; magnetic minerals determined from the TMA data are goethite and/or ferromagnetic iron hydroxides of the goethite type, hemoilmenite (HI), titanomagnetite (TM), magnetite (MT), titanohematite (TH), metallic iron (Fe) and ferrospinel (FS); and M_t/M_o is the ratio of the magnetization upon heating of a sample to 800°C to its initial value.

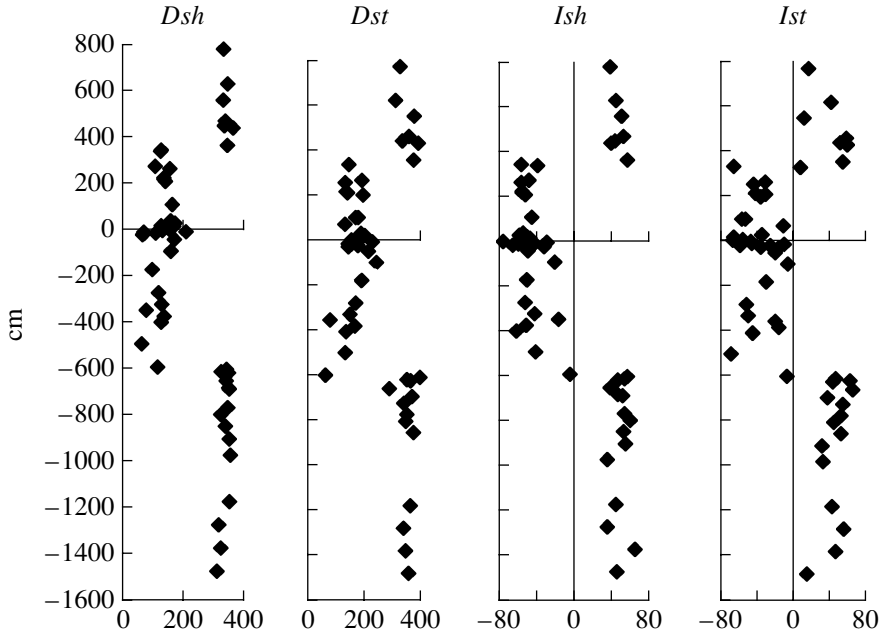

Fig. 7. Magnetostratigraphic columns from the data of AF demagnetization (declination *Dsh* and inclination *Ish*) and thermal demagnetization (*Dst* and *Ist*).

This leads to a decrease in M_{rs}/M_s. As a result, points in the Day diagram are displaced downward to the right.

PALEOMAGNETIC RESULTS

The AF and thermal demagnetization of samples revealed a stable component of the *NRM* M_n. Due to the very small value of M_n, the AF demagnetization could be conducted only to 35–40 mT, and the thermal demagnetization, to 400°C; a large scatter is observed above these fields and temperature because the measured values of M_n are close to the sensitivity threshold of the JR-4 magnetometer, and the magnetic bias effect becomes appreciable.

As shown in the petromagnetic part of the paper, the main carriers of remanence and, in particular, *NRM* are titanomagnetite grains in the Danian sediments and magnetite grains in the Maastrichtian sediments; the patterns of the along-section titanohematite distribution and *NRM* behavior are rather similar. The along-section distributions of other magnetic minerals differ sharply from the *NRM* behavior. Although the concentrations of goethite and ilmenite in the sediments are rather high, their magnetization is two to three orders lower compared to titanomagnetite and magnetite, while the concentration of highly magnetic iron is lower than the concentrations of titanomagnetite and magnetite by an order of magnitude. Accordingly, their contribution to the *NRM* is unobservable. Titanomagnetite grains of volcanic origin are potential carriers of the depositional, i.e., primary, magnetization, and this may also be stated concerning magnetite grains of detrital and/or volcanic origin.

The main contribution of titanomagnetite and magnetite to the *NRM* is supported by the very close results of AF and thermal demagnetizations and, which is most important, the coincidence of magnetic polarities, as well as the boundaries of the chron *C*29*r*, in all samples (Fig. 7). Whereas thermal demagnetization results can be affected by the contribution of highly coercive iron hydroxides and hemoilmenite, thermal demagnetization to temperatures above 300°C completely eliminates their contribution to the *NRM*.

As seen from Fig. 7, the scatter in thermal demagnetization results is appreciably wider, implying a higher quality of the AF demagnetization, so that further estimates are derived from the AF demagnetization results. The AF and thermal demagnetization data reveal a distinct magnetostratigraphic pattern: a magnetic zone of reversed polarity, namely, the chron *C*29*r*, is clearly resolved in the section. Its lower boundary is pinpointed by sample t29 (–590 cm) and upper boundary —by sample t11 (345 cm), and both boundaries are recorded as minimums of M_n/M_{rs} (Fig. 8c). The presence of the minimums indicates, first, high paleomagnetic reliability of the inferred primary *NRM* component and, second, the absence of noticeable breaks near the *C*29*r* chron boundaries. Another, even stronger argument for the primary nature of M_n (more specifically, of its polarity) is the global magnetostratigraphic correlation of this interval with a number of sections, both continental, such as Gubbio (Italy) [Rocchia et al., 1990], and oceanic [Pechersky and Garbuzenko, 2005]. Average paleomagnetic directions for the intervals of normal and reversed polarity (Table 3) differ from 180°C. The difference between directions of normal

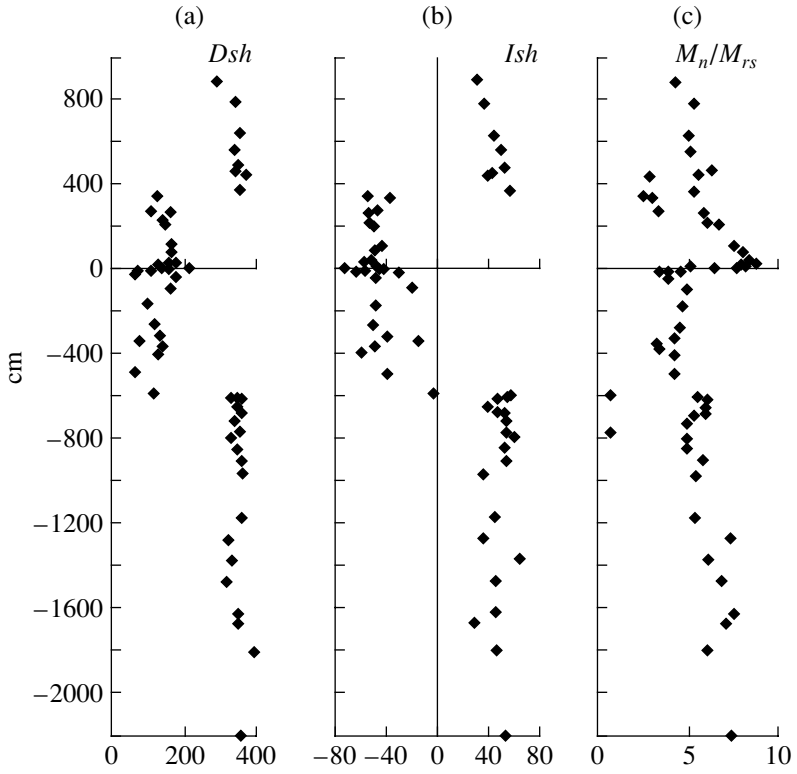

Fig. 8. Magnetostratigraphy of the Tetritskaro section: (a, b) inclination (a) and declination (b) of the NRM stable part after AF demagnetization in stratigraphic coordinates; (c) ratio (on a logarithmic scale) of the stable part of M_n (after AF demagnetization to 20–30 mT) to the saturation remanence M_{rs} characterizing relative variations in the paleointensity.

and reversed polarity amounts to $\gamma = 14.8°$ for the upper *N* zone, with its admissible critical value being $\gamma_{cr} = 18.9°$ (i.e., this difference is insignificant and the reversal test is positive), and $\gamma = 23.6°$ for the lower *N* zone with its admissible critical value of $\gamma_{cr} = 12.8$, i.e., in this case the difference is significant and the reversal test is negative [McFadden and McElhinny, 1990]. Comparing paleomagnetic directions of normal and

Table 3. Paleomagnetic directions and pole coordinates from the Tetritskaro data

Zone	*n*	*Ds*/*Dg*	*Is*/*Ig*	*K*	α95	*P*	Φ	Λ	*dp*	*dm*
*N*1	8	347.6	46.6	82.2	6.7	27.9	73.4	264.6	5.5	6.8
		333.8	54.5	25.3	11.2		68.2	305.8	6.7	9.4
R	29	139.5	–52.2	8.7	10.7	32.8	–56.9	131.9	9.7	14.5
		120.4	–50.4	8.5	10.8		–42.1	140.9	9.7	14.5
*N*2	19	356.0	47.9	29.4	6.3	29	77.5	239.4	5.4	8.2
		338.9	55.1	30.3	6.2		73.0	301.3	6.3	8.8
Sum	56	341.6	50.4	15.5	5.3	31.3	72.2	285.2	4.8	7.1
		322.6	54.7	15.5	5.3		60.6	313.8	5.3	7.5
Europe, 65 Ma							80.7	197.4		

Note: Magnetic zones of the Tetritskaro section (Fig. 9) in the first column are upper (normal polarity *N*), middle (reversed polarity *R*, chron C29r), and lower (normal polarity *N*) zones; *n* is the number of samples (section levels) used for the calculation of the average direction; *Ds* and *Is* are the declination and inclination of the stable *NRM* component in stratigraphic coordinates (upper rows); *Dg* and *Ig* are its declination and inclination in geographic coordinates (lower rows); *K* is the precision parameter of paleomagnetic directions; α95 is the 95% confidence radius; *P* is the paleolatitude determined from the paleomagnetic inclination; Φ and Λ are the latitude and longitude of the paleomagnetic pole calculated from the paleomagnetic direction at the point (41°N, 43°E); *dp* and *dm* are the semiaxis of the 95% confidence oval; and the bottom row presents the paleomagnetic pole coordinates for stable Europe of the latest Cretaceous–earliest Paleogene [Besse and Courtillot, 2002].

reversed polarity, we clearly see that the former are shifted relative to the latter (rotated through 180°) toward the direction of the contemporary geomagnetic field, which is likely due to incomplete demagnetization of the samples (Table 3); this problem is settled, to an extent, by the reversal method, i.e., by adding the directions of normal and reversed polarity.

Our task does not include magnetotectonic analysis of paleomagnetic directions and poles; here we only note that the Tetritskaro pole differs from the synchronous pole of stable Europe (Table 3) because, in the latest Cretaceous–earliest Paleogene, the Trans-Caucasian territory was located to the south from its present position with respect to the southern margin of the East European plate, and the block including the Tetritskaro section was rotated counterclockwise through about 20°.

In the geomagnetic polarity time scale [Cande and Kent, 1995], chron *C*29*r* covers the 0.83-Myr long interval from 65.58 to 64.75 Ma. In the Tetritskaro section, magnetic zone *C*29*r* covers a 935-m thick interval (Fig. 8). Accordingly, the average sedimentation rate in this interval of the section can be estimated at 1.126 cm/kyr [Cande and Kent, 1995]. The distance between the K/T boundary and the lower boundary of the chron is 590 cm. Given the above average rate of sedimentation, the age of the boundary layer, i.e., the biostratigraphic K/T boundary, is 65.06 Ma, which is very close to the generally acknowledged age of Mesozoic/Cenozoic boundary estimated at 65 Ma.

The polarity change intervals are the same at both the lower and upper boundaries of the chron *C*29*r* and amount to less than 20 cm, which corresponds to a time interval of less than 15 kyr; a more accurate determination is impossible due to insufficiently detailed sampling. The lower transitional zone is fixed more reliably: sample 29a (–600 cm) yields the normal polarity (D_{st} = 334°, I_{st} = 58°) and the normal ratio M_n/M_{rs} = 1.31×10^{-3} (Fig. 8), whereas sample 29 (–590 cm) coincides with the transition itself (D_{st} = 118°, I_{st} = –1°) and is pinpointed by a sharp minimum, $M_n/M_{rs} = 0.14\text{x}10^{-3}$. Such a pattern points to the absence of a noticeable break in sedimentation near the boundaries of chron *C*29*r*.

The paleointensity (M_n/M_{rs}) outside the *C*29*r* chron is at approximately the same level (Fig. 8c) and, below the R chron smoothly decreases from 2–3 at the base of the section to 1–1.5 $\times$ 10^{-3} near the chron, whereas M_n/M_{rs} is close to 1×10^{-3} in the lower half of the chron and above it. However, near the K/T boundary, beginning from –2 cm, the ratio M_n/M_{rs} rises in a jumpwise manner to 4–5 $\times$ 10^{-3} and then smoothly decreases to the preceding level. Appreciable oscillations in the direction observed in the narrow interval from –15 to + 2 cm are better expressed in the declination (Figs. 8a, 8b). Thus, the geomagnetic polarity change does not coincide with the K/T boundary, which however is fixed by an abrupt rise in the paleointensity and, to a lesser extent, by oscillations in the field direction.

Considering that the section is lithologically rather homogeneous, an average sedimentation rate of 1.126 cm/kyr can be taken for the entire section studied. Then, we obtain that the section encompasses a time interval of 2.75 Myr. The accumulation time of the boundary clay layer, averaging in thickness 2 cm, is about 1.8 kyr, and sharp variations in the paleointensity and direction of the geomagnetic field encompass an interval of 30–40 kyr. Such an accumulation time of clay near the base of which shock-metamorphic quartz grains and anomalously high Ir concentrations have been discovered and, moreover, the length of the time interval of sharp variations in the intensity and direction of the field cannot be related to a short-term impact event.

CONCLUSIONS

(A) The boundary layer in the Tetritskaro section is pinpointed *primarily by an abrupt rise in the paramagnetic magnetization, i.e., by the total concentration of iron*, and, to a lesser degree, by the rise in concentrations of such magnetic minerals as goethite, hemoilmenite, hematite, and magnetite. The along-section distributions of titanomagnetite (evidently, of volcanic origin) and metallic iron (evidently, of cosmic origin) are not controlled by the K/T boundary or lithology of the sediments. A similar pattern was observed in the previously studied Gams, Teplovka, and Koshak sections [Pechersky et al., 2006a, 2006b; Molostovsky et al., 2006].

A global natures of accumulation of iron hydroxides at the K/T boundary is supported by their synchronous accumulation at least within Europe, as is evident from magnetostratigraphic data: the K/T boundary is positioned inside the chron *C*29*r* almost at the same level in the sections Gubbio (Italy) [Rocchia et al., 1990], Gams (Austria) [Mauritsch, 1986], and Tetritskaro (Georgia).

Such a consistent phenomenon at the boundary of geological eras cannot be explained in terms of local physiographic features of the sedimentation process; rather, the short-term iron accumulation event is similar to the formation of metalliferous sediments, i.e., related to a global short-term activation of hydrothermal–volcanic processes caused, for example, by intense plume magmatism.

(B) The Mesozoic/Cenozoic boundary is distinguished by an abrupt rise in the paleointensity of the geomagnetic field and instability of paleomagnetic directions rather than by a polarity change. The accumulation time of the boundary clay layer averaging in thickness 2 cm is 1.8 kyr, and sharp variations in the paleointensity and direction of the geomagnetic field encompass an interval of about 30–40 kyr. These times (even the accumulation time of clay showing impact features) cannot be related to such a short-term event as the impact of a large meteorite.

REFERENCES

1. Sh. Adamia., N. Salukvadze, M. Nazarov, et al., "Geological Events at the Cretaceous–Paleogene Boundary in Georgia (Caucasus)," Geol. Carpath. **23** (3), 35–43 (1993).
2. W. Alvarez, A. Asaro, and A. Montanari, "Iridium Profile for 10 Million Years across the Cretaceous–Tertiary Boundary at Gubbio (Italy)," Science **250**, 1700–1703 (1990).
3. V. I. Bagin, T. I. Gendler, L. G. Dainyak, and A. V. Sukhorada, "Thermal Transformations in Biotite," Fiz. Zemli, No. 9, 66–76 (1976).
4. V. I. Bagin, T. I. Gendler, L. G. Dainyak, and A. V. Sukhorada, "Stability of Magnetic Products of Biotite Decomposition," Fiz. Zemli, No. 2, 71–78 (1977).
5. V. I. Bagin, T. S. Gendler, and T. A. Avilova, *Magnetism α-Oxides and Hydroxides of Iron* (IFZ AN SSSR, Moscow, 1988) [in Russian].
6. J. Besse and V. Courtillot, "Apparent and True Polar Wander and Geometry of the Geomagnetic Field over the Last 200 Myr," J. Geophys. Res. **107** (2002).
7. B. V. Burov, D. K. Nourgaliev, and P. G. Yasonov, *Paleomagnetic Analysis* (KGU, Kazan, 1986) [in Russian].
8. S. C. Cande and D. V. Kent, "Revised Calibration of the Geomagnetic Polarity Time Scale for the Late Cretaceous and Cenozoic, J. Geophys. Res. **100**, 6093–6095 (1995).
9. R. Day, M. Fuller and V. A. Schmidt, "Hysteresis Properties of Titanomagnetites: Grain-Size and Compositional Dependence," Phys. Earth Planet. Inter. **13** 260–266 (1977).
10. D. J. Dunlop, "Theory and Application of the Day Plot (M_{rs}/M_s versus H_{cr}/H_c). 1. Theoretical Curves and Tests Using Titanomagnetite Data," J. Geophys. Res. **107**, 10.1029/2001JB000486 (2002a).
11. D. J. Dunlop, "Theory and Application of the Day Plot (M_{rs}/M_s vs. H_{cr}/H_c). 2. Application to Data for Rocks, Sediments and Soils, J. Geophys. Res. **107**, 10.1029/2001JB000487 (2002b).
12. B. D. Ellwood, W. D. MacDonald, C. Wheeler, and S. L. Benoist, "The K–T Boundary in Oman: Identified Using Magnetic Susceptibility Field Measurements with Geochemical Information," Earth Planet. Sci. Lett. **206**, 529–540 (2003).
13. R. E. Ernst and K. L. Buchan, "Recognizing Mantle Plumes in the Geological Record," Annu. Rev. Earth Planet. Sci. **31**, 469–523 (2003).
14. A. K. Gapeev and V. A. Tselmovich, "Microstructure and Composition Natural and Synthetic Titanomagnetites That Experienced Multiphase Oxidation," Fiz. Zemli, No. 10, 42–49 (1988).
15. A. F. Grachev, O. A. Korchagin, H. A. Kollmann, et al., "A New Look at the Nature of the Transitional Layer at the K/T Boundary near Gams, Eastern Alps, Austria, and the Problem of the Mass Extinction of the Bota," Russ. J. Earth Sci. **7**, ES6001. doi: 10.2205/2005ES000189 (2005).
16. F. M. Gradstein, J. Ogg, and A. G. Smith, *A Geological Time Scale* (Univ. Press, Cambridge, 2004).
17. H. J. Mauritsch, "Der Stand der Palaomagnetischen Forschung in den Ostaplen," Leobner Hefte fur Angewandte Geophys. **1**, 141–160 (1986).
18. P. L. McFadden and M. McElhinny, "Classification of Reversal Test in Paleomagnetism, Geophys. J. Int. **103**, 725–729 (1990).
19. E. A. Molostovsky, V. A. Fomin, and D. M. Pechersky, "Sedimentogenesis in Maastrichtian–Danian Basins of the Russian Plate and Adjacent Areas in the Context of Plume Geodynamics," Russ. J. Earth Sci. **8**, ES6001. doi: 10.2205/2006ES000206 (2006).
20. T. Nagata, *Rock-Magnetism* (Maruzen, Tokyo, 1961; IL, Moscow, 1965) [in Russian].
21. D. M. Pechersky, D. K. Nourgaliev, and Z. V. Sharonova, "Magnetolithologic and Magnetomineralogical Characteristics of Sediments at the Mesozoic/Cenozoic Boundary: The Koshak Section (Mangyshlak Peninsula)," Fiz. Zemli, No. 11, 99–112 (2006) [Izvestiya, Phys. Solid Earth **42**, 957–970 (2006)].
22. D. M. Pechersky and A. V. Garbuzenko, "The Mesozoic–Cenozoic Boundary: Paleomagnetic Characteristic, Russ. J. Earth Sci. **7** (2) (2005).
23. D. M. Pechersky, A. F. Grachev, D. K. Nourgaliev, et al., "Magnetolithologic and Magnetomineralogical Characteristics of Deposits at the Mesozoic/Cenozoic Boundary: Gams Section (Austria)," Russ. J. Earth Sci. (2006).
24. C. Richter C. and B. A. Van der Pluijm, "Separation of Paramagnetic and Ferrimagnetic Susceptibilities Using Low Temperature Magnetic Susceptibilities and Comparison with High Field Methods," Phys. Earth Planet. Int. **822**, 111–121 (1994).
25. R. Rocchia, D. Boclet, Ph. Bonte, et al., "The Cretaceous–Tertiary Boundary at Gubbio Revisited: Vertical Extent of the Ir Anomaly," Earth Planet. Sci. Lett. **99**, 206–219 (1990).
26. P. Rochette, M. Jackson, and C. Aubourg, "Rock Magnetism and Interpretation of Anisotropy of Magnetic Susceptibility, Rev. Geophys. **30**, 209-226 (1992).
27. A. B. Veimarn, D. P. Naidin, L. F. Kopaevich, et al., *Global Catastrophic Events and Implications for Stratigraphic Correlations of Sedimentary Basins of Various Types* (MGU, Moscow, 1998) [in Russian].
28. P. G. Yasonov, D. K. Nourgaliev, B. V. Bourov, and F. Heller, "A Modernized Coercivity Spectrometer," Geol. Carpath. **49** (3), 224–226 (1998).